JOURNAL OF AIRCRAFT
Vol. 39, No. 2, March–April 2002

High-Speed Civil Transport Design Space Exploration Using Aerodynamic Response Surface Approximations

Chuck A. Baker,* Bernard Grossman,† Raphael T. Haftka,‡ William H. Mason,§ and Layne T. Watson¶
Virginia Polytechnic Institute and State University, Blacksburg, Virginia 24061-0203

A method has been developed to generate and use polynomial approximations to the range and cruise drag components in a highly constrained, multidisciplinary design optimization of a high-speed civil transport (HSCT) configuration. The method improves optimization performance by eliminating the numerical noise present in the analyses through the use of response surface methodology. In this implementation quadratic polynomials are fit within variable bounds to data gathered from a series of numerical analyses of different aircraft designs. Because the HSCT optimization process contains noise and suffers from a nonconvex design space even when noise is filtered out, multiple optimization runs are performed from different starting points with and without the response surface models in order to evaluate both their effectiveness as surrogate functions and as a design exploration tool. The alternative method used is variable complexity modeling (VCM). It is shown that response surface methodology facilitates design space exploration, allowing improvements in terms of both convergence performance and computational effort when multiple starting points are required, although using VCM usually produces better final designs.

Introduction

NUMERICAL noise is a critical issue in the field of multidisciplinary design optimization (MDO). Numerical noise occurs as a result of the incomplete convergence of iterative processes, round-off errors, the nature of adaptive numerical algorithms, and the discrete representation of continuous physical objects.[1,2] Such numerical noise is typically manifested as a low-amplitude, high-frequency variation in the results obtained from computer analyses as the design parameters vary. When gradient-based numerical optimization is attempted, this oscillatory behavior results in numerous, artificial local optima and causes slow convergence or even convergence failures.[1,3]

In the MDO of a high-speed civil transport (HSCT), numerical noise is present in the analyses of various disciplines, with the majority of the noise originating from aerodynamic computations. In our studies numerical noise was most evident in the calculation of drag coefficients, which subsequently led to noise in the calculation of range.

Previous work using a variable complexity modeling (VCM) approach[3–6] encountered the noise problem and was only partially successful in solving it. This approach used computationally efficient low-fidelity models and computationally expensive high-fidelity models in a method that reduced the computational effort to an acceptable level. The low-fidelity models were also less noisy. At each optimization cycle the low-fidelity predictions were corrected using a scaling factor obtained from the expensive methods. The VCM approach was successful in reducing CPU time and jumping over some of the artificial local minima caused by noise, but occasionally failed because erratic calculations of scaling factors at the peaks and troughs of the noise lead to convergence problems. VCM is also used in this study as a comparison to the response surface methodology (RSM) employed.

A somewhat different approach to numerical noise is Kelly's implicit filtering,[7] which has been very successful for low-dimensional problems where the noise can be characterized with constant parameters. Its application to MDO problems where the noise characteristics vary across the constraints and across the design space is not so clear, but its performance on low-dimensional HSCT MDO problems is comparable to that of response surfaces.[8]

More recent work to eliminate the noise employs RSM. RSM[9–11] uses simple mathematical models, typically low-order polynomials, to approximate the response and smooth out numerical noise present in the analyses. Such response-surface (RS) models are created using a limited number of analyses at a set of statistically selected points in the design space. The time consumed by running these initial analyses is considered an investment in the future use of the RS models, with the understanding that the optimization performance will be increased enough for the RS models to be beneficial if a certain number of optimizations are executed. This is important because many optimization runs are needed to study the possibility of local optima occurring in a high-dimensional design space.

HSCT optimizations have been conducted using aerodynamic RS models for smaller regions of the design space with success.[12] The purpose of this work is to construct RS models that cover a larger volume of the design space and evaluate the effectiveness of these models as a design space exploration tool by running a local optimizer from a wide variety of starting points.

HSCT Design Problem

The design problem considered is the optimization of a HSCT configuration[13,14] to minimize takeoff gross weight (TOGW) for a range of 5500 n miles and a cruise Mach number of 2.4 while carrying 251 passengers. The choice of gross weight as the objective function directly incorporates both aerodynamic and structural considerations in that the structural design directly affects aircraft empty weight and drag, whereas aerodynamic performance dictates drag and thus the required fuel weight.

Received 17 April 1999; revision received 12 February 2001; accepted for publication 30 April 2001.

*Graduate Research Assistant, Department of Aerospace and Ocean Engineering, Multidisciplinary Analysis and Design (MAD) Center for Advanced Vehicles.

†Professor and Department Head of Aerospace and Ocean Engineering, Multidisciplinary Analysis and Design (MAD) Center for Advanced Vehicles. Associate Fellow AIAA.

‡Professor, Department of Aerospace Engineering, Mechanics and Engineering Science, University of Florida, Gainesville, FL 32611-6250. Fellow AIAA.

§Professor of Aerospace and Ocean Engineering, Multidisciplinary Analysis and Design (MAD) Center for Advanced Vehicles. Associate Fellow AIAA.

¶Professor of Computer Science and Mathematics, Multidisciplinary Analysis and Design (MAD) Center for Advanced Vehicles.

Table 1 HSCT configuration design variables

No.	Description
1	Wing root chord, ft
2	Leading-edge (LE) break, x, ft
3	LE break, y, ft
4	Trailing-edge (TE) break, x, ft
5	LE wing tip, x, ft
6	Wing tip chord, ft
7	Wing semispan, ft
8	Location airfoil maximum thickness
9	LE radius parameter
10	t/c at wing root
11	t/c at LE break
12	t/c at wing tip
13	Fuselage axial restraint #1, ft
14	Fuselage radius at axial restraint #1, ft
15	Fuselage axial restraint #2, ft
16	Fuselage radius at axial restraint #2, ft
17	Fuselage axial restraint #3, ft
18	Fuselage radius at axial restraint #3, ft
19	Fuselage axial restraint #4, ft
20	Fuselage radius at axial restraint #4, ft
21	Location of inboard nacelle, ft
22	Location of outboard nacelle, ft
23	Mission fuel weight, lb
24	Starting cruise altitude, ft
25	Cruise climb rate, ft/min
26	Vertical tail area, ft^2
27	Horizontal tail area, ft^2
28	Thrust per engine, lb

Table 2 HSCT optimization constraints

No.	Description
1	Range $\geq$ 5500 n miles
2	Required C_L at landing speed $\leq$1
2–20	Sectiion $C_1 \leq 2$
21	Landing angle of attack $\leq$12 deg
22	Fuel volume $\leq$ half of wing volume
23	Spike prevention
24–41	Wing chord $\geq$7.0 ft
42–43	No engine scrape at landing angle of attack
44–45	No engine scrape at landing angle of attack, with 5-deg roll
46	No wing tip scrape at landing
47	Rudder deflection for crosswind landing $\leq$22.5 deg
48	Bank angle for crosswind landing $\leq$5 deg
49	Takeoff rotation to occur $\leq$5 s
50	Tail deflection for approach trim $\leq$22.5 deg
51	Wing root TE $\leq$ horizontal tail LE
52	Balanced field length $\leq$11,000 ft
53	TE break scrape at landing with 5-deg roll
54	LE break $\leq$ semispan
55	TE break $\leq$ semispan
56–58	Root, break, tip $t/c \geq 1.5\%$
59	Fuselage: $x_{\text{rest1}} \geq 5$ ft
60	Fuselage: $x_{\text{rest1}} + 10 \text{ ft} \leq x_{\text{rest2}}$
61	Fuselage: $x_{\text{rest2}} + 10 \text{ ft} \leq x_{\text{rest3}}$
62	Fuselage: $x_{\text{rest3}} + 10 \text{ ft} \leq x_{\text{rest4}}$
63	Fuselage: $x_{\text{rest4}} + 10 \text{ ft} \leq 300$ ft
64	Nacelle 1, $y \geq$ side of body
65	Nacelle 1, $y \leq$ nacelle 2, y
66	Engine-out limit with vertical tail design; otherwise 50%
67–68	Maximum thrust required $\leq$ available thrust

To perform aircraft configuration optimization successfully, it is important to have a simple, but meaningful, mathematical characterization of the geometry of the aircraft. This paper uses a model that defines the HSCT design problem using the 28 design variables listed in Table 1. Twenty-four of the design variables describe the geometry of the aircraft and can be divided into six categories: wing planform, airfoil shape, tail areas, nacelle placement, and fuselage shape. In addition to the geometric parameters, four variables define the idealized cruise mission: mission fuel, engine thrust, initial cruise altitude, and constant climb rate used in the range calculation.

Sixty-eight geometry, performance, and aerodynamic constraints, listed in Table 2, are included in the optimization. Aerodynamic and performance constraints can only be assessed after a complete analysis of the HSCT design; however, the geometric constraints can be evaluated using algebraic relations based on the 24 geometric design variables. It is in the evaluation of the range constraint using the aerodynamic analyses where the numerical noise is evident.

The analysis methods used to calculate the three main contributors to the drag components ($C_{D\text{wave}}$, $C_{L\alpha}$, and C_T/C_L^2) used in the drag calculation and their corresponding ranges are described in Refs. 4, 5, and 15. The aerodynamic calculations are based on the Mach box method[16,17] and the Harris wave drag code.[18] A simple strip boundary-layer friction estimate is implemented as in Ref. 5. A vortex lattice method[19] with vortex lift and ground effects included[20] is used to calculate landing angle of attack.

All calculations were performed on an SGI Power Challenge. Optimizations used the modified method of Feasible Directions (MMFD) algorithm in the optimization software package DOT.[21] If the RS model optimum design violates the range constraint calculated by exact analyses by a small amount, it is sometimes possible to add fuel to the aircraft to increase the range without violating any other constraints. When this is done, the aircraft TOGW used for comparison is replaced by the corrected TOGW (CTOGW) that includes the added fuel weight.

Variable Complexity Modeling

The two variable complexity modeling approximations used in this study are scaled approximations and global-local approximations (GLA). With scaled approximations a scaling function $\sigma(\boldsymbol{x})$ is calculated as

$$\sigma(\boldsymbol{x}_0) = \frac{f_{\text{hf}}(\boldsymbol{x}_0)}{f_{\text{lf}}(\boldsymbol{x}_0)} \tag{1}$$

where $f_{\text{hf}}(\boldsymbol{x}_0)$ represents a high-fidelity analysis result and $f_{\text{lf}}(\boldsymbol{x}_0)$ represents a low-fidelity analysis result, both evaluated at a specific design point $\boldsymbol{x}_0$ at the beginning of an optimization cycle (a single DOT MMFD optimization run with move limits imposed). During an optimization cycle, the scaled approximate analysis results, $f(\boldsymbol{x})$ are calculated as

$$f(\boldsymbol{x}) \approx \sigma(\boldsymbol{x}_0) f_{\text{lf}}(\boldsymbol{x}) \tag{2}$$

Instead of keeping the scaling factor constant, the GLA uses a scaling function of the form

$$\sigma(\boldsymbol{x}) \approx \sigma(\boldsymbol{x}_0) + \nabla\sigma(\boldsymbol{x} - \boldsymbol{x}_0) \tag{3}$$

The gradient of σ at $\boldsymbol{x}_0$ is performed by forward differences involving both f_{hf} and f_{lf}. For each approximation method the scaled simple analysis is used throughout the cycle until convergence. Then a new value of the scale factor is computed, and the optimization is repeated. The scaled approximation is employed only when analysis noise makes the derivative-based methods, like GLA, intractable. In optimization runs using RS models, VCM is used for the calculation of low-speed aerodynamic and takeoff parameters.

During each optimization cycle, limits are placed on the optimizer to prevent large errors in the approximations. First, each cycle is run with tight move limits. This prevents the optimizer from moving far away from its initial point, where the approximations may become inaccurate. Second, because some of the low-fidelity models are based on planform idealizations[22] restrictions are implemented to prevent the optimizer from investigating designs where these assumptions are violated.

Construction of RS Models

The RSM process begins with the selection of a central (or baseline) design. The central design becomes the centroid of a 28-dimensional box over which the RS model is created. The central design for this work was chosen to be an optimum design that was achieved using VCM. The initial (starting point A) and optimal planform shapes are shown in Fig. 1.

The next step in the RSM process involves the definition of variable bounds. Ideally the bounds would be selected to provide a large

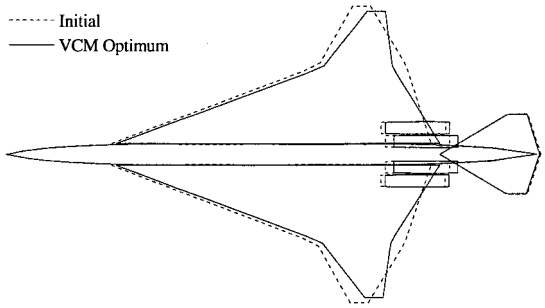

Fig. 1 Planform shapes for VCM optimization run (starting pt. A).

volume to allow a wide variation in the design parameters. However, as the design box becomes large the error in the quadratic RS model also grows. The goal here is to have a design box that provides a significant amount of variation in designs while keeping RS errors, the difference between a value calculated using the exact analyses and the RS models, acceptable. For this study the variable bounds were set at ±15% of the baseline values of each design variable.

With the design box defined, a sample set of designs is generated. Initially, two different methods were used in the construction of the data set. One of the data sets is created using an orthogonal array generator developed by Owen (private communication), which implements a method by Bose[23] consisting of 47 levels for a total of 2209 points. The other data set is a 2105 point SCD[11] consisting mostly of design box vertices [a 2048 small composite design (SCD) plus face points and the central design]. The number of points in each design set is then slightly decreased by the removal of geometrically impossible designs. The impossible designs include configurations with negative chords that arise from a combination of extreme design variable values that occurs at certain vertices of the design box. Only three designs were removed from the 2209-point orthogonal array, whereas 512 were eliminated from the 2105-point SCD-based data set caused by the presence of a large number of points at the vertices where negative wing chords occur. Because such a large number of points were removed from the SCD, an additional 1024-point SCD was created for a box with ±7.5% variable bounds, providing a second level of points. The total number of points remaining was 2206 for the orthogonal array and 2617 for the SCD-based set after pruning the sets to exclude impossible designs.

Once the design set has been pruned, the analyses are run for each point, and the RS models can be generated. A total of four RS models are generated for the aerodynamics. Because the noise is seen primarily in the range constraint, it was decided to approach this problem from two directions: to model the range itself as a function of the 28 design variables and to model the individual drag components used to calculate the range as a function of the 28 design variables. The aerodynamic calculations took 597 CPU minutes to analyze the 2206-point set and 685 CPU min for the 2617-point set on the Power Challenge.

The statistical analysis software (SAS)[24] is used to create all of the RS models, which are quadratic least-square fits of the sample design set data. A quadratic polynomial was used because its simple form accurately models the behavior of the response, and it has a relatively low number of coefficients that need to be found, reducing the number of data points needed. The quadratic response surface model has the form

$$y = c_0 + \sum_{1 \le j \le 28} c_j x_j + \sum_{1 \le j \le k \le 28} c_{jk} x_j x_k \qquad (4)$$

where y is the response; the x_j are the design variables; and c_0, c_j, and c_{jk} are the polynomial coefficients.

The error of each RS model's range calculated at the design points is listed in Table 3. As can be seen from the table, the orthogonal array RS models have smaller errors compared to those of the SCD set. For this reason the orthogonal array RS models were selected for use in this optimization study.

Table 3 Errors of RS models

Error, n miles	Orthogonal array		SCD-based data set	
	Range RS	Drag RS range	Range RS	Drag RS range
Median	24	17	39	21
rms	46	31	63	36

Table 4 Performance data for VCM and RS model optimization runs (starting pt. A)

Head	Initial	VCM optimum	Range RS optimum	Drag RS optimum
Range, RS, n miles	——	——	5,500	5,500
Range, exact, n miles	5,607	5,500	5,522	5,481
TOGW, lb	805,955	750,350	768,859	761,836
CTOGW, lb	——	750,350	766,879	763,546
CPU time, min.	——	184	45	30
Active side constraints	——	None	None	None

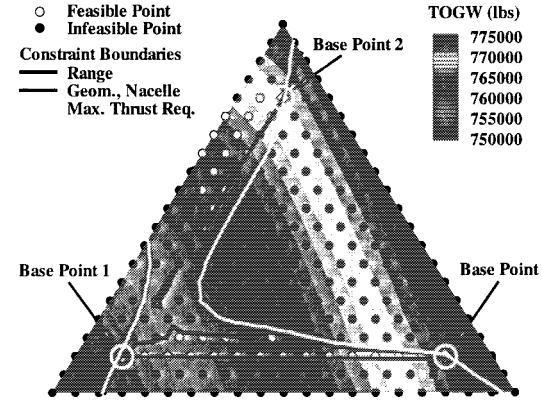

Fig. 2 Design space visualization plot.

In previous work it was observed that multiple optima existed even when smooth RS models were used.[25] A visualization technique was needed to view the topology of the design space to understand the cause of the local optima; however, the dimensionality of the design prevents traditional techniques from being used. One of the design space visualization methods that was developed is shown in Fig. 2. To construct this plot, three different feasible base point designs are chosen. The base points are connected to form a plane in 28-dimensional space, and a grid is created in this plane. The values for the objective function and constraints, using RS models, are then calculated at each grid point.

This plot shows that even in this plane the design space is complicated and nonconvex. The range constraint, calculated from the drag RS models, appears to be multiply connected (though it is actually connected in the 28-dimensional space), providing three possible locations for local optima.

Optimization from Multiple Starting Points

The first RS model optimization run was conducted from starting point A, the same starting point as the VCM optimization that produced the central design. The performance data for these optimizations are listed in Table 4. The resulting planform shapes and convergence histories are shown in Figs. 3 and 4, respectively.

For the optimum designs the range RS model overpredicted the exact range by 22 n miles, and the range calculated using drag RS models was 19 miles short of the exact range. The sets of models yielded a slightly heavier optimum and used only 25% of the time needed for the VCM optimization. If a drag RS model optimization run is restarted from the VCM optimum, the optimizer is able to converge at a feasible design similar to the VCM optimum, weighing 752,810 lb. The VCM optimization takes twice as many

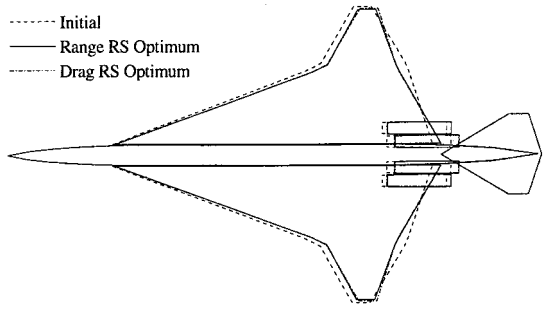

Fig. 3 Planform shapes for RS model optimization runs (starting pt. A).

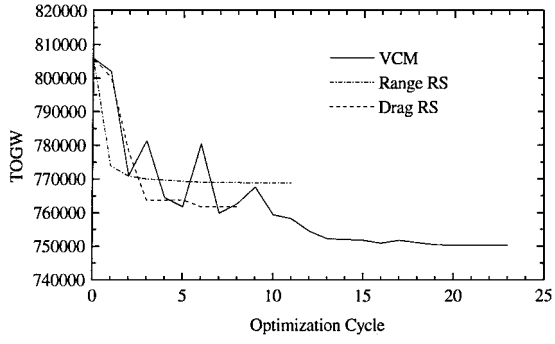

Fig. 4 Convergence histories for optimization runs (starting pt. A).

cycles to converge, and the cycles are twice as long as a result of the multifidelity calculations. The convergence history of the VCM also shows a slow, noisy convergence when compared to those of the RS models.

Because of the different methods of calculating range between RSM and VCM, the design spaces also look different. This explains why the RSM optimization restarted from the VCM optimum does not converge to the same design. The optimizer sees a different value for range through RSM and finds its own optimum accordingly. The exact range, or the range used by VCM, may not be the true range. As mentioned before, noise can cause peaks and troughs, with the true range possibly being some average between adjacent extremes. VCM can take advantage of the troughs in the noise and resultingly use a lower value than the true range.

For the remainder of the optimization runs, the single-range RS model was abandoned in favor of the drag RS models. This was done to simplify comparison of the results, providing a single RS optimum for every VCM optimum. The drag RS models were chosen because they had slightly smaller errors (Table 3) and because it was felt that the individual drag components are better modeled by a quadratic function of the 28 design variables than their resulting range.

A total of four more starting points were used to explore the design space. The starting points were selected primarily for their variety, with starting point B representing a conventional HSCT design and the other points being considerably more unorthodox. Details of optimizations from starting points B, C, D, and E are shown in Figs. 5–12 and Tables 5–8.

Starting points B and C resulted in essentially the same optimum design independently of the method used. The discrepancies in the optimum weights can be attributed to small differences in the optimal airfoil design variables.

The optimum designs obtained from starting point D show a little more diversity between them and are by far the lightest designs achieved. The biggest difference in these two designs is the size of the horizontal tail. The RS model optimum has a much larger horizontal tail and is consequentially much heavier. Other notable differences between these two designs are the length of the root chord and the sweep of the outboard section of the wing.

For starting points A and E the VCM and RS model optimum designs have very different weights. The only major difference seen

Table 5 Performance data for VCM and RS model optimization runs (starting pt. B)

Head	Initial	VCM optimum	Drag RS optimum
Range, RS, n miles	——	——	5,500
Range, Exact, n miles	4,946	5,500	5,463
TOGW, lb	823,331	791,066	789,386
CTOGW, lb	——	791,066	792,716
CPU time, min.	——	326	56
Active side constraints	——	None	None

Table 6 Performance data for VCM and RS model optimization runs (starting pt. C)

Head	Initial	VCM optimum	Drag RS optimum
Range, RS, n miles	——	——	5,500
Range, exact, n miles	4,621	5,500	5,478
TOGW, lb	795,161	765,751	756,515
CTOGW, lb	——	765,751	758,495
CPU time, min.	——	293	98
Active side constraints	——	Maximum vert. tail area	Maximum vert. tail area

Table 7 Performance data for VCM and RS model optimization runs (starting pt. D)

Head	Initial	VCM optimum	Drag RS optimum
Range, RS, n miles	——	——	5,500
Range, exact, n miles	5,295	5,500	5,472
TOGW, lb	872,763	733,785	743,431
CTOGW, lb	——	733,785	745,951
CPU time, min.	——	218	51
Active side constraints	——	None	None

Table 8 Performance data for VCM and RS model optimization runs (starting pt. E)

Head	Initial	VCM optimum	Drag RS optimum
Range, RS, n miles	——	——	5,500
Range, Exact, n miles	4,316	5,500	5,464
TOGW, lb	769,080	766,249	770,256
CTOGW, lb	——	766,249	773,496
CPU time, min.	——	146	44
Active side constraints	——	None	None

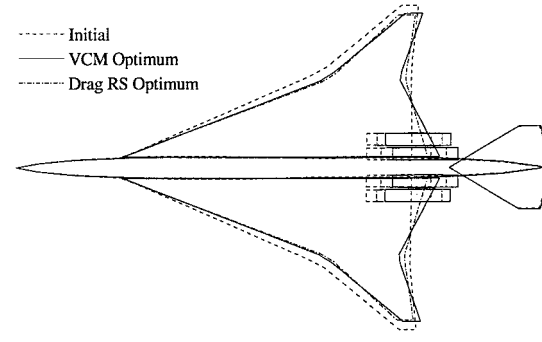

Fig. 5 Planform shapes for VCM and RS model optimization runs (starting pt. B).

in designs is the sweep of the outboard section of the wing. In both cases the RS model converges at a design that has an outboard sweep angle roughly halfway between that of the initial and optimal VCM design. This difference leads to the RS model designs being more than 10,000 lb heavier than the VCM optimum.

Again, a distinct difference between the two methods can be seen in the convergence history and CPU time used for each optimization. In all cases the optimization using RS models moved swiftly and

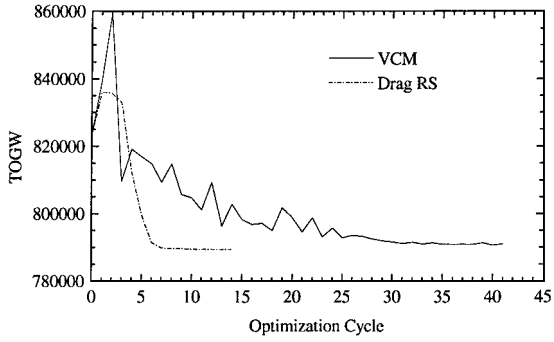

Fig. 6 Convergence histories for optimization runs (starting pt. B).

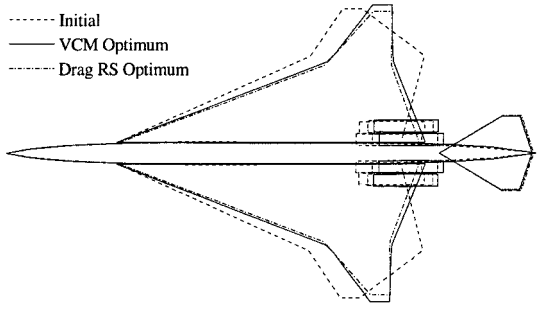

Fig. 7 Planform shapes for VCM and RS model optimization runs (starting pt. C).

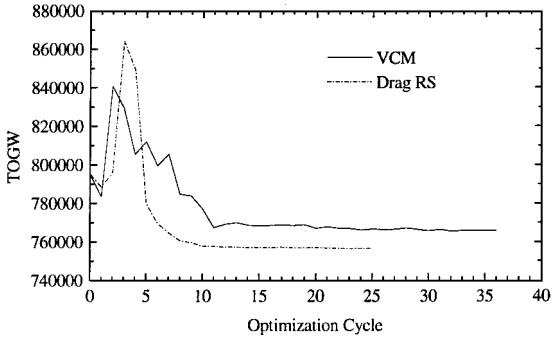

Fig. 8 Convergence histories for optimization runs (starting pt. C).

smoothly to their optimum while the VCM approach's convergence is visibly hindered by the presence of noise. Because of the smooth convergence and short function evaluation time, the RS model optimizations converged 76% faster on average, in terms of CPU time, than the VCM optimizations.

The drag RS models also proved to be highly accurate in all of the optimizations. The maximum error seen in the range calculated using the drag RS models at any of the optima was only 37 n miles.

From all of the starting points, the optimizer was successful in overcoming a large initial range deficit to produce a lighter, feasible design whether using the VCM approach or RS models. The best optimum design for each method came from starting point D, where the VCM approach produced a design with a TOGW of 733,785 lb and the RS models produced a design with a TOGW of 745,951 lb.

Discussion

In the five HSCT configuration optimizations that were performed, we were able to see the advantages and disadvantages of quadratic RS models for the design box used. In our implementation RSM has the advantage of accurate noise filtering and computational efficiency over the VCM approach when using a sufficient number of starting points. However, the VCM approach has the advantage of not being confined to a design box as well as the ability to jump through the design space toward promising regions. Also

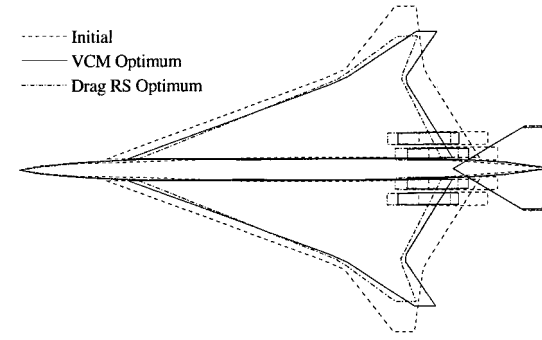

Fig. 9 Planform shapes for VCM and RS model optimization runs (starting pt. D).

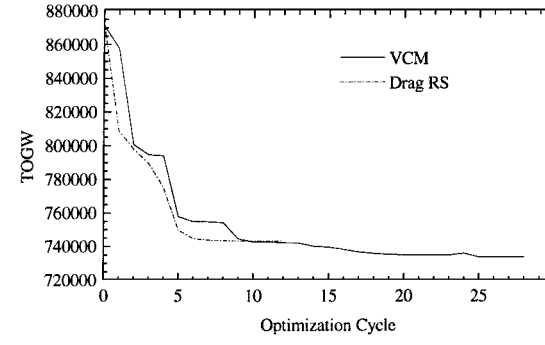

Fig. 10 Convergence histories for optimization runs (starting pt. D).

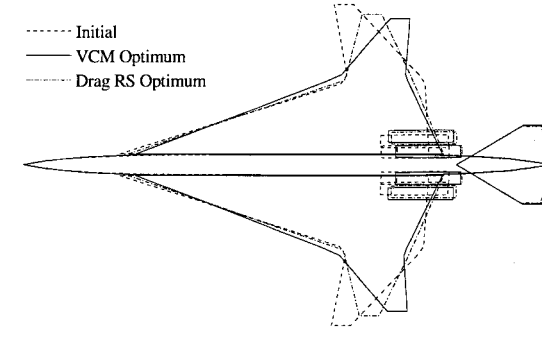

Fig. 11 Planform shapes for VCM and RS model optimization runs (starting pt. E).

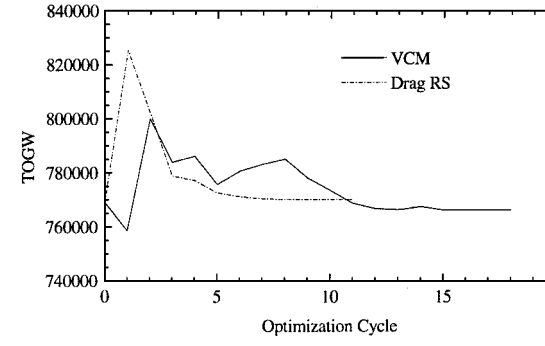

Fig. 12 Convergence histories for optimization runs (starting pt. E).

if the design box had been made sufficiently larger, it is likely that the quadratic response surface models would have been inaccurate enough to render them ineffective.

The values of range predicted by the drag RS models were exceptionally accurate over the entire design box. The RS models were also able to capture the governing trends of the exact values of range (excluding the noise) because most of the optimizations started from the same initial design were able to find very similar

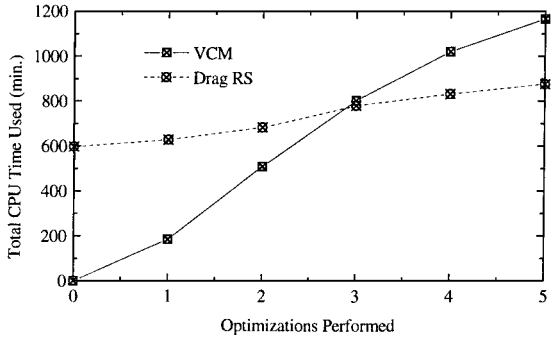

Fig. 13 Comparison of total CPU time used for VCM and RS model optimizations.

optimum designs whether the VCM approach or RS models were used.

The biggest advantage in using the RS models for design space exploration is not necessarily in the optimum that is found but in how efficiently this optimum is found. Even though there is an initial investment of almost 600 CPU minutes required for the construction of the RS models, the increase in optimization performance using the RS models over the five optimization runs from different starting conditions can be seen in Fig. 13. In this case after three optimizations were performed, the total CPU time used by RS model optimizations was surpassed by that of conventional optimizations using VCM.

Although the results were virtually identical for starting point B and starting point C, the VCM optimization is able to make substantial improvements over the RS models for the other three starting points. These improvements are most likely caused by the behavior of the VCM approach during an individual optimization cycle. Because VCM uses low-fidelity analyses with some initially calculated correction factor, it is possible, as each optimization cycle progresses, for it to jump through constraints that exist in the high-fidelity analyses and RS models. For example, the RS model optimization from starting point A begins by following the path of the VCM optimization until the RS models encounter a local minimum caused by the range constraint. The VCM optimization continues on to reduce the weight by an additional 13,000 lb to converge at an optimal weight of 750,350 lb. When the RS model optimization run is restarted from the VCM optimum, it converges at a design weighing 752,810 lb. In this case the VCM approach was able to move to a region of the design space that is better than what it originally started in, but the RSM was not.

Conclusions

The use of RS models in this study was valuable in providing a relatively quick and accurate means of exploring the design space. The large size of the design box that was used is evident in the variety of initial designs that were available for optimization. The spaciousness of the design box can also be seen in that the side constraints did not play an important role in the optimization process.

When performing design space exploration in a nonconvex space without the aid of a global optimizer, multiple starting points are required with or without RS models. In this case the RSM used was successful in filtering out the effects of noise while providing savings of almost 5 hours of CPU time when compared to the VCM approach. Alternatively, the VCM approach was successful in navigating to better regions of the design space.

Acknowledgment

Support for this research effort was provided through the NASA Langley Research Center Grants NAG1-1160 and NAG1-1562.

References

[1]Giunta, A. A., Balabanov, V., Haim, D., Grossman, B., Mason, W. H., Watson, L. T., and Haftka, R. T., "Multidisciplinary Optimisation of a Supersonic Transport Using Design of Experiments Theory and Response Surface Modelling," *The Aeronautical Journal of the Royal Aeronautical Society*, Vol. 101, No. 1008, 1997, pp. 347–356.

[2]Venter, G., Haftka, R. T., and Starnes, J. H., "Construction of Response Surface Approximation for Design Optimization," *AIAA Journal*, Vol. 36, No. 12, 1998, pp. 2242–2249.

[3]Dudley, J., Huang, X., MacMillin, P. E., Grossman, B., Haftka, R. T., and Mason, W. H., "Multidisciplinary Optimization of the High-Speed Civil Transport," AIAA Paper 95-0124, Jan. 1995.

[4]Hutchison, M. G., Unger, E. R., Mason, W. H., Grossman, B., and Haftka, R. T., "Aerodynamic Optimization of an HSCT Configuration Using Variable-Complexity Modeling," AIAA Paper 93-0101, Jan. 1993.

[5]Hutchison, M. G., Unger, E. R., Mason, W. H., Grossman, B., and Haftka, R. T., "Variable-Complexity Aerodynamic Optimization of a High-Speed Civil Transport Wing," *Journal of Aircraft*, Vol. 31, No. 1, 1994, pp. 110–116.

[6]Dudley, J., Huang, X., Haftka, R. T., Grossman, B., and Mason, W. H., "Variable-Complexity Interlacing of Weight Equation and Structural Optimization of the High-Speed Civil Transport," AIAA Paper 94-4377, Sept. 1994.

[7]Gilmore, P., and Kelley, C. T., "An Implicit Filtering Algorithm for Optimization of Functions with Many Local Minima," *SIAM Journal on Optimization*, Vol. 5, No. 2, 1995, pp. 269–285.

[8]Giunta, A. A., "Aircraft Multidisciplinary Design Optimization Using Design of Experiments Theory and Response Surface Modeling Methods," Ph.D. Dissertation, Dept. of Aerospace and Ocean Engineering, Virginia Polytechnic Inst. and State Univ., Blacksburg, VA, May 1997.

[9]Box, G. E. P., and Wilson, K. B., "On the Experimental Attainment of Optimum Conditions," *Journal of Royal Statistical Society*, Vol. B13, No. 1, 1951, pp. 38–45.

[10]Box, G. E. P., Hunter, W. G., and Hunter, J. S., *Statistics for Experimenters: An Introduction to Design, Data Analysis, and Model Building*, Wiley, New York, 1978, pp. 78–83.

[11]Myers, R. H., and Montgomery, D. C., *Response Surface Methodology: Process and Product Optimization Using Designed Experiments*, Wiley, New York, 1995, pp. 650, 651.

[12]Golovidov, O., "Variable-Complexity Response Surface Approximations for Aerodynamic Parameters in HSCT Optimization," Multidisciplinary Analysis and Design Center for Advanced Vehicles, Virginia Polytechnic Inst. and State Univ., Rept. 97-06-01, Blacksburg, VA, June 1997.

[13]MacMillin, P., Golovidov, O., Mason, W., Grossman, B., and Haftka, R., "Trim, Control and Performance Effects in Variable-Complexity High-Speed Civil Transport Design," Multidisciplinary Analysis and Design Center for Advanced Vehicles, Virginia Polytechnic Inst. and State Univ., Rept. 96-07-01, Blacksburg, VA, July 1996.

[14]MacMillin, P. E., Golovidov, O. B., Mason, W. H., Grossman, B., and Haftka, R. T., "An MDO Investigation of the Impact of Practical Constraints on an HSCT Optimization," AIAA Paper 97-0098, Jan. 1997.

[15]Hutchison, M. G., Unger, E., Mason, W. H., Grossman, B., and Haftka, R. T., "Variable-Complexity Aerodynamic Optimization of a High Speed Civil Transport Wing," *Journal of Aircraft*, Vol. 31, No. 1, 1994, pp. 110–116.

[16]Carlson, H., Mack, R., and Barger, R., "Estimation of Attainable Leading Edge Thrust for Wings at Subsonic and Supersonic Speeds," NASA TP-1500, Oct. 1979.

[17]Carlson, H., and Miller, D., "Numerical Methods for the Design and Analysis of Wings at Supersonic Speeds," NASA TN D-7713, Dec. 1974.

[18]Harris, R. V., Jr., "An Analysis and Correlation of Aircraft Wave Drag," NASA TM X-947, March 1964.

[19]Bertin, J., and Smith, M., *Aerodynamics for Engineers*, 2nd ed., Prentice–Hall, Upper Saddle River, NJ, 1989, pp. 261–282.

[20]Hutchison, M. G., "Multidisciplinary Optimization of High-Speed Civil Transport Configurations Using Variable-Complexity Modeling," Ph.D. Dissertation, Dept. of Aerospace and Ocean Engineering, Virginia Polytechnic Inst. and State Univ., Blacksburg, VA, May 1993.

[21]*DOT Users Manual*, Version 4.20, Vanderplaats Research and Development, Inc., Colorado Springs, CO, 1995.

[22]Cohen, D., and Friedman, M. D., "Theoretical Investigation of the Supersonic Lift and Drag of Thin, Sweptback Wings with Increased Sweep Near the Root," NACA TN-2959, 1953.

[23]Bose, R. C., "On the Application of the Properties of Galois Fields to the Problem of Construction of Hyper-Graeco-Latin Squares," *The Indian Journal of Statistics*, Vol. 3, Pt. 4, 1938, pp. 323–338.

[24]*SAS/STAT User's Guide*, Version 6, SAS Inst., Inc., Cary, NC, 1995.

[25]Knill, D. L., Giunta, A. A., Baker, C. A., Grossman, B., Mason, W. H., Haftka, R. T., and Watson, L. T., "Response Surface Models Combining Linear and Euler Aerodynamics for Supersonic Transport Design," *Journal of Aircraft*, Vol. 36, No. 1., 1999, pp. 75–86.